Nucleic Acids Research, 2025, **53**, gkaf813
https://doi.org/10.1093/nar/gkaf813
Nucleic Acid Enzymes

Evidence human FTO catalyses hydroxylation of *N*^{6}-methyladenosine without direct formation of a demethylated product contrasting with ALKBH5/2/3 and bacterial AlkB

Simranjeet Kaur[1,†], Pratheesh Maheswaran[2,†], Samanpreet Kaur[2], Yingqi Lai[1], Eidarus Salah[2], Dong Zhang[2], Shifali Shishodia[2,3,*], Christopher J. Schofield[2,*], Wei Shen Aik[1,*]

[1]Department of Chemistry, Hong Kong Baptist University, Kowloon Tong, Hong Kong SAR, China
[2]The Department of Chemistry and the Ineos Oxford Institute for Antimicrobial Research, Chemistry Research Laboratory, University of Oxford, 12 Mansfield Road, Oxford OX1 3TA, United Kingdom
[3]Present address: California Institute for Biomedical Research, La Jolla, CA 92037, United States

[*]To whom correspondence should be addressed. Email: aikweishen@hkbu.edu.hk
Correspondence may also be addressed to Christopher J. Schofield. Email: christopher.schofield@chem.ox.ac.uk
Correspondence may also be addressed to Shifali Shishodia. Email: sshishodia@scripps.edu
[†]The first two authors should be regarded as Joint First Authors.

Abstract

N^6-Methyladenosine (m^{6}A) is a prevalent post-transcriptional modification in eukaryotic messenger RNA. Two cancer-linked human Fe(II) and 2-oxoglutarate (2OG)-dependent oxygenases, the fat mass and obesity associated-protein (FTO), and AlkB human homolog 5 (ALKBH5) catalyse m^{6}A methyl group oxidation. While ALKBH5 has consistently been reported to catalyse m^{6}A demethylation, there are conflicting reports concerning the FTO products. We report studies using mass spectrometry and nuclear magnetic resonance comparing products of FTO, ALKBH5, and DNA damage repair demethylases (human ALKBH2 and ALKBH3 and bacterial AlkB, using m^{1}A single-stranded DNA substrates). The results with m^{6}A-containing single-stranded RNA (ssRNA) and *N*^{6},2′-*O*-dimethyladenosine adjacent to the 5′ m^{7}G triphosphate cap ssRNA substrates imply that the predominant FTO product is *N*^{6}-hydroxymethyladenosine, either with or without methylation on the substrate ribose 2′-hydroxyl group. The nascent hemiaminal product undergoes relatively slow non-enzyme catalysed fragmentation giving adenosine/formaldehyde. The other four 2OG-dependent oxygenases tested, including ALKBH5, produce demethylated bases as the predominant products. The results imply that, at least in isolated form, FTO preferentially acts as a hydroxylase, producing a hemiaminal product, rather than a demethylase, distinguishing it from ALKBH5. They highlight a need for investigations into the roles of hemiaminal-type modifications to nucleic acids, in both healthy biology and disease.

Graphical abstract

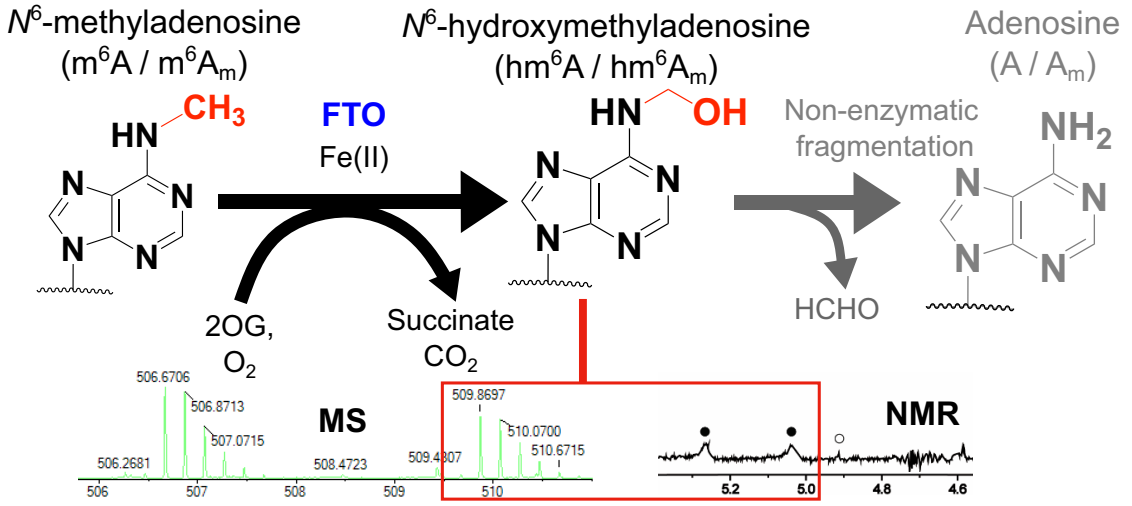

Received: March 17, 2025. **Revised:** June 12, 2025. **Editorial Decision:** July 13, 2025. **Accepted:** August 7, 2025

Introduction

Methylation of messenger RNA (mRNA) is a common post-transcriptional modification that has roles in regulating mRNA function. Two important sites of mRNA methylation involve adenosine, i.e. internal N^6-methyladenosine (m^6A) and N^6,2′-*O*-dimethyladenosine (m^6A_m), in the 5′ mRNA cap [1–5]. The internal m^6A mark is located within the RR(m^6A)CH consensus motif (R: G/A; H: A/C/U) [6, 7], while m^6A_m modifications commonly occur in the nucleotide adjacent to the 5′ N^7-methylguanosine (m^7G) triphosphate cap [4, 8, 9].

Although multiple human N^{ε}-methyl lysine histone demethylases (KDMs) have been identified [10–13], only two human oxygenases modifying the methyl group of m^6A have been identified [14, 15], namely the fat mass and obesity associated-protein (FTO) [14, 16] and AlkB homolog 5 (ALKBH5) [15]. FTO and ALKBH5 are related by sequence and structure, and both are linked to cancer [17–22]; mutations of the *FTO* gene are also linked to other diseases, including obesity and brain disorders [23–26]. FTO is reported to catalyse demethylation of the 5′-cap m^6A_m [27, 28]; ALKBH5, however, is reported to be inactive against m^6A_m [29, 30]. Despite the biological importance of FTO and ALKBH5, as evidenced by cellular and genetic studies, how the reactions that they catalyse are connected to healthy development/physiology and disease is poorly understood.

Both FTO and ALKBH5 are Fe(II) and 2-oxoglutarate (2OG)-dependent oxygenases that employ 2OG and O_2 as co-substrates to oxidize m^6A, producing succinate, CO_2, and formaldehyde (HCHO) as co-products [16, 31–34]. There are 60–70 human 2OG oxygenases [34–36], which, *inter alia*, play important roles in collagen biosynthesis [37], lipid metabolism [38], epigenetic regulation [39, 40], the hypoxic response [41], and DNA damage repair [40, 42]. In the latter case, human homologues (ALKBH2, ALKBH3) of bacterial AlkB are reported to catalyse damage repair via oxidation of DNA-damaging alkylations, resulting in fragmentation to give an aldehyde and the repaired base (Fig. 1D) [43–46]. Some 2OG oxygenases (e.g. AlkB [40, 42, 44, 47]) manifest broad substrate and product selectivities, but this is not always the case [31].

Interestingly, there is evidence that FTO and ALKBH5 produce different products with the same m^6A-containing substrates [33, 48, 49]. When reacted with m^6A-containing ssRNA in the presence of Fe(II) and 2OG, FTO has been reported to produce not only N^6-demethylated adenosine but also hm^6A, N^6-formyladenosine (f^6A), and N^6-methyleneadenosine (imine) [32, 33, 49]; by contrast, ALKBH5 has been reported to produce only N^6-demethylated adenosine [33, 48, 50] (Fig. 1A–C). Crystal structures of ALKBH5–m^6A RNA complexes have led to a proposed mechanism for ALKBH5-catalysed hm^6A fragmentation, which is promoted by a proton shuttling machinery involving $Lys132_{ALKBH5}$ and $Tyr139_{ALKBH5}$, a mechanism not apparent in the FTO active site [48, 50].

Studies on the reactions of HCHO with canonical and modified nucleobases have shown that HCHO reacts with endocyclic nitrogens to give equivalent hemiaminal products, as observed with thymidine and uridine monophosphates [49]. Such endocyclic reactions of HCHO are faster than with exocyclic nitrogens; however, the exocyclic hemiaminal adducts, as formed with guanine, cytosine, and, in particular, adenine, are more stable in solution [49]. FTO-catalysed hydroxylation of the m^6A nucleoside (m^6A [^{13}C]-labelled on its 6-methyl group) was shown to give hm^6A as the major product as observed by nuclear magnetic resonance (NMR); by contrast, (3-methyl)thymidine was observed to undergo demethylation, consistent with the decreased stability of the likely endocyclic hemiaminal intermediate in the case of (3-methyl)thymidine demethylation compared to the analogous exocyclic hemiaminals [49]; this work did not describe comparative studies with ALKBH5 [49, 51].

Some reported methods used to analyse FTO products/mRNA modification might not preserve hm^6A/hm^6A_m adducts and other hemiaminal-type covalent modifications that are relatively unstable in aqueous environments [14, 32, 33, 52–54]. Here, we report studies using high-resolution mass spectrometry (MS) and real-time NMR to analyse modifications to m^6A-containing ssRNA produced as a consequence of FTO and ALKBH5 catalysis, comparing the results with those for the apparent *bona fide* demethylases ALKBH2, ALKBH3, and bacterial AlkB. The combined results clearly demonstrate that, in contrast to the other tested oxygenases, isolated FTO preferentially acts as a hydroxylase rather than a demethylase, highlighting a need for further investigations into the biological roles of hm^6A and hm^6A_m.

Materials and methods

Production and purification of FTO, FTOΔ31, $ALKBH5_{66–292}$, $ALKBH5_{74–292}$, $ALKBH5_{74–292}$ K132E, AlkBΔN11, ALKBH2, and ALKBH3 recombinant proteins

Recombinant forms of FTO [54], FTOΔ31 [48, 55], $ALKBH5_{66–292}$ [56], $ALKBH5_{74–292}$ [48], and $ALKBH5_{74–292}$ K132E [48] were produced as previously reported. DNA constructs containing AlkBΔN11, full-length ALKBH2, and full-length ALKBH3 were cloned into the pET-28a(+) vector using the NcoI and BamHI, NdeI and NcoI, and NcoI and HindIII restriction sites, respectively. In brief, *Escherichia coli* BL21 (DE3) cells were transformed with the respective expression vectors and grown in LB medium at 37°C with shaking until the culture reached an optical density at 600 nm (OD_{600}) of 0.6–0.8. Protein production was induced by the addition of isopropyl β-D-1-thiogalactopyranoside (IPTG) to a final concentration of 0.5 mM. The cell cultures were incubated at 18°C with shaking at 150–180 rpm for ∼18 h. The cells were harvested by centrifugation (8000 rpm, 10 min, 4°C); the resulting pellets were stored at −80°C. Frozen cell pellets were resuspended in lysis buffer (20 mM Tris–HCl, pH 7.5, 500 mM NaCl, and 10 mM imidazole) supplemented with 1 mg DNase I and a cOmplete™ protease inhibitor cocktail (Roche) and lysed by sonication on ice. The lysates were then cleared by centrifugation (20 000 rpm for 30 min, 4°C), and the supernatant was loaded onto a 5-ml HisTrap HP column (GE Healthcare) pre-equilibrated with binding buffer (20 mM Tris–HCl, pH 7.5, 500 mM NaCl, and 10 mM imidazole). The column was washed with wash buffer (20 mM Tris–HCl, pH 7.5, 500 mM NaCl, and 40 mM imidazole) and eluted with elution buffer (20 mM Tris–HCl, pH 7.5, 500 mM NaCl, and 500 mM imidazole). The eluted protein was further purified using a Superdex 75 300-ml column (Cytiva) pre-equilibrated

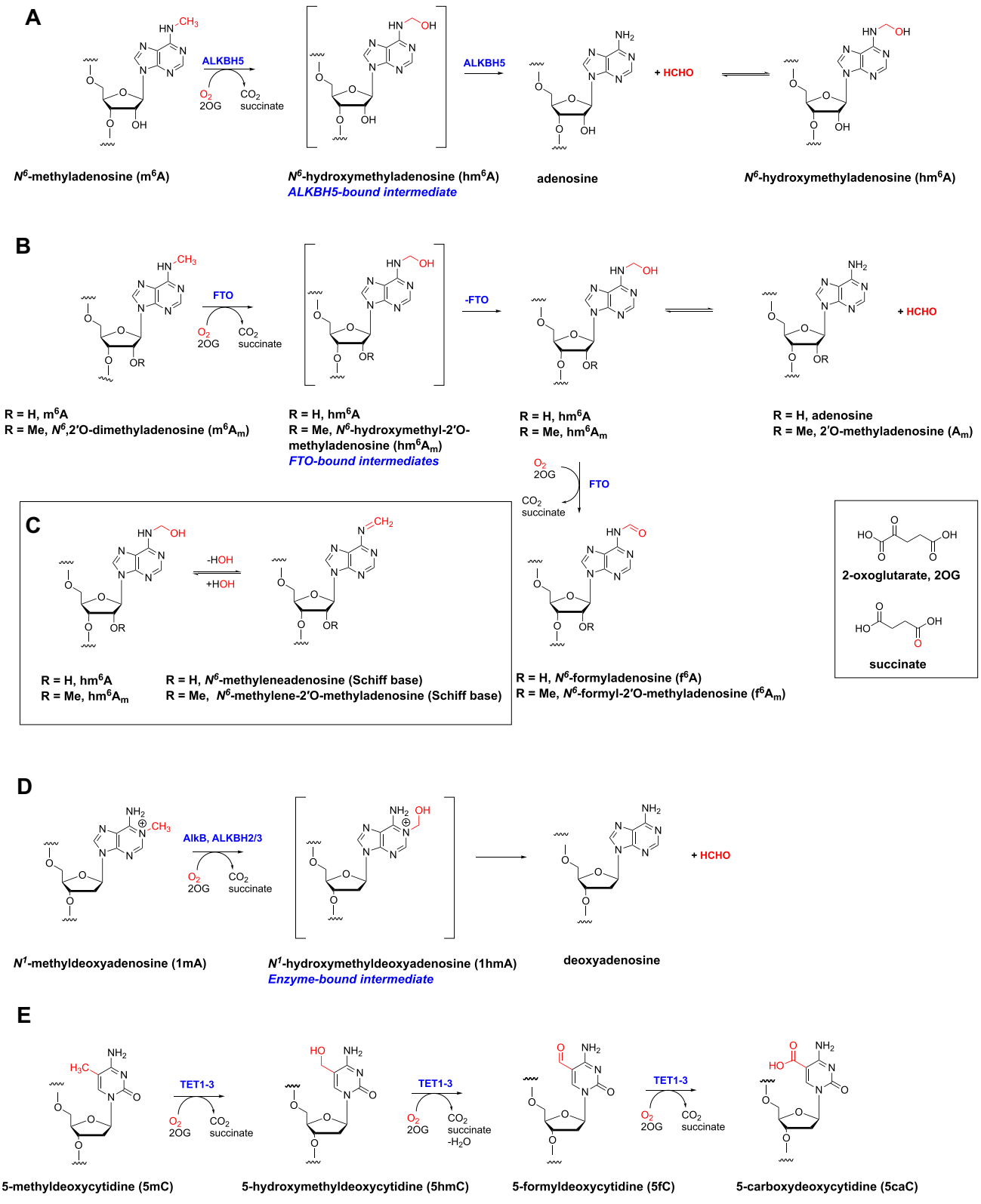

Figure 1. Reactions reported to be catalysed by ALKBH5 and FTO and related human 2OG-dependent oxygenases. Reactions catalysed by (**A**) ALKBH5, (**B**, **C**) FTO, (**D**) AlkB, ALKBH2/3, and (**E**) TET1-3 are shown. Note that ALKBH5 is proposed to catalyse demethylation via a transient enzyme-bound N^6-hydroxymethyladenosine (hm^6A) intermediate. In the case of FTO, in addition to demethylated adenosine, evidence has been reported for additional products, i.e. hm^6A, an imine, and f^6A. Note that tautomeric states other than those shown may be relevant.

with buffer containing 50 mM Tris–HCl (pH 7.5) and 150 mM NaCl.

Quadrupole Time-of-Flight Mass Spectrometry (QTOF-MS)-based *in vitro* m^6A_m and m^6A hydroxylation assays

Reaction mixtures containing 0.5 μM FTOΔ31, 0.5 μM $ALKBH5_{74–292}$ or $ALKBH5_{74–292}$ K132E, 20 μM $m^7Gpppm^6A_mUACUU$ ssRNA substrate (Biosynthesis, USA) or $UGGm^6ACUGC$ ssRNA (Horizon Discovery), 200 μM 2OG disodium salt, 100 μM diammonium Fe(II) sulfate, 1 mM sodium L-ascorbate, and with or without 25 μM 2,4-PDCA inhibitor (for $ALKBH5_{74–292}$ and $ALKBH5_{74–292}$ K132E) in 25 mM Tris (pH 7.2) were prepared and incubated at 37°C. Reactions were sampled at various time points between 0 and 45 min, then purified using C-18 Ziptips (Thermo Fisher) (purification time = 5 min), and immediately snap-frozen and stored in liquid nitrogen. The samples were later thawed and subjected to QTOF-MS analysis (SCIEX Triple TOF 6600). For data acquisition, the sample [in 50% (v/v) MeCN] was injected directly into the spectrometer at 30 μl/min. One hundred to one hundred twenty scans were accumulated in the negative mode, and total ion count was used to quantify the signal ion intensities. Data analysis was performed by the Sciex OS Explorer software. The plots were generated using GraphPad Prism 10.1.1.

QTOF-MS-based hm^6A_m and hm^6A decay assays

Initial hydroxylation reactions were initiated by preparing reaction mixtures as described above with incubation at 37°C for 10 min (hm^6A_m) or 30 min (hm^6A). The mixture was then divided equally. A final concentration of 1 mM FTO inhibitor 2,4-PDCA [55–57] was added to one of the portions, 1 mM; an equivalent volume of reaction buffer was added to the other portion. The samples were incubated at 37°C and sampled every 45 min until 450 min. They were then purified using C-18 Ziptips (Thermo Fisher) (purification time = 5 min) and immediately snap-frozen and stored in liquid nitrogen. The samples were later thawed and subjected to QTOF-MS analysis (SCIEX Triple TOF 6600). Procedures for data acquisition, processing, and analysis were as described for the QTOF-MS-based *in vitro* m^6A_m and m^6A hydroxylation assays. Data analyses were performed using GraphPad Prism 10.

Ion-pairing reversed-phase liquid chromatography–mass spectrometry time-course assays

Solutions containing His_6-tagged enzyme [FTO (0.25 or 0.5 μM), ALKBH5 (2 or 4 or 8 μM), or AlkBΔN11 (0.2 μM)/ALKBH2 (0.5 μM)/ALKBH3 (0.5 μM)], 100 μM sodium-L-ascorbate (500 μM for ALKBH5), 10 μM ammonium iron(II) sulfate hydrate (50 μM for ALKBH5), and 10 μM 2OG disodium salt (50 μM for ALKBH5) was added to 20 μM of substrate in 50 mM HEPES buffer and 0.1% (v/v) Tween 20 (pH 7.5) (230 μl final reaction volume). 30 μl of the mixture extract was taken at each time point and quenched by adding 60 μl of 1.33% (v/v) aqueous acetic acid for LC/MS analysis. Samples were transferred to an Eppendorf vial, then frozen using liquid nitrogen and stored at −20°C. Prior to MS analysis, samples were thawed and centrifuged (14 000 rpm, 20 min, 4°C); 10 μl was used for analysis. $UGGm^6ACUGC$ (ssRNA, 8-mer) was obtained from Dharmacon custom RNA synthesis (Horizon Discovery). $AAAGCAGm^1AAATTCGAAAAAGCGAA$ (ssDNA, 24-mer) and CAm^1AAT (ssDNA, 5-mer) were obtained from Keck Oligos. The dried oligonucleotides were reconstituted to 1 mM and diluted to 200 μM in UltraPure DNase/RNase-free distilled water.

A Waters® ACQUITY UPLC Oligonucleotide BEH C18 Column (130 Å, 1.7 μm, 2.1 mm × 50 mm) with a gradient of 98% (v/v) buffer A to 70% (v/v) buffer B over 8 min at room temperature was used for purification. Buffer A: 200 mM HFIP, 8.15 mM Triethylamine (TEA) buffer, and 5% (v/v) methanol. Buffer B: 20% (v/v) buffer A + 80% (v/v) methanol. The LC/MS system was operated using MassLynx™ version 4.1 (Waters Corp., Milford, MA, USA). LC/MS chromatograms were acquired in the negative ion full scan mode using an ESI-MS capillary voltage of 2.5–3.0 kV, a sample cone voltage of 40 V, and an MCP detector voltage of 3000 V. The desolvation gas flow rate was 800 l/h. The cone gas flow rate was set to 30 l/h. The desolvation temperature and source temperature were set to 400°C and 150°C, respectively. Relevant molecular ions were extracted, and the reaction progress curve was plotted using GraphPad Prism 5.

NMR monitoring of FTO and ALKBH5 using ^{13}C-labelled m^6A nucleoside as substrate

The ^{13}C-m^6A nucleoside with N^6-methyl group selectively labelled with ^{13}C was synthesized as reported [49]. The FTO-catalysed reaction was monitored using both ^1H NMR and the gradient-selected 1D heteronuclear single quantum correlation (^1H–^{13}C-HSQC) method. In brief, samples containing FTO or ALKBH5 (20 μM, final concentration, final reaction volume: 160 μl; enzymes were stored in Tris buffer), ^{13}C-m^6A (400 μM), 2OG (5 mM), sodium L-ascorbate (1 mM), and Fe(II) ammonium sulfate (20 μM) in ammonium formate buffer in D_2O (pD 7.9) were mixed and immediately transferred to a 3-mm-diameter MATCH NMR tube (Hilgenberg). The time lag between sample mixing and the first acquisition completion was 15 min. Spectra were acquired using 1D NOESY water pre-saturation (Bruker pulse program: *noesygppr1d*) using 160 scans and a relaxation delay of 2 s, and 1D ^1H–^{13}C-HSQC (Bruker pulse program: hsqcgpclip1d) using 400 scans with a relaxation delay of 2 s. The HSQC was optimized for a $^1J_{CH}$ coupling of 145 Hz. NMR spectra were measured using a Bruker AVIII 700 MHz NMR spectrometer equipped with a TCI helium cooled cryoprobe. Data were processed with TopSpin v.3.5.6. The temperature of the probe was 310 K. The time course was run for 720 min.

HPLC-based m^6A nucleoside hydroxylation assays

Reaction mixtures containing 10 μM FTO, 100 μM N^6-methyladenosine (m^6A) nucleoside substrate, 200 μM 2OG disodium salt, 100 μM diammonium Fe(II) sulfate, and 1 mM sodium L-ascorbate in 25 mM Tris (pH 7.2) were prepared in a final volume of 50 μl and incubated at 37°C for 5 min. Reactions were quenched by heating the mixture at 90 °C for 5 min. Fifty microlitres of methanol was then added, and the mixtures were centrifuged to remove the precipitated protein. The mixtures were injected into an Agilent Technologies 1200 Infinity high-performance liquid chromatography (HPLC) equipped with a UV detector. The product (adenosine) and substrate (m^6A) were separated using an Agilent 5 HC C18(2), 250 mm × 4.6 mm column, at a flow rate of

0.5 ml/min. The UV detector was set at a wavelength of 254 nm. The mobile phase consisted of H_2O with 0.1% trifluoroacetic acid (TFA) as buffer A and acetonitrile with 0.1% TFA as buffer B. The gradient program was as follows: 0–20 min, 2%–4% B; 20–40 min, 4%–8% B; 40–41 min, 8%–100% B; and 41–55 min, 100% B. UV peaks were integrated using MestReNova 14.2.3. For the determination of the K_M of m^6A nucleoside, assays were conducted in triplicate across a range of substrate concentrations (80 μM, 160 μM, 320 μM, 640 μM, 1.28 mM, 2.56 mM, 5.12 mM, and 10.24 mM). The K_M value was calculated from the Michaelis–Menten model using GraphPad Prism 10.1.1.

NMR monitoring of FTO and ALKBH5 using a 5-mer m^6A-containing ssRNA as substrate

m^6A phosphoramidite and GGm^6ACU were synthesized as reported [58, 59]. Reactions contained FTO or ALKBH5 (20 μM), ssRNA GGm^6ACU (200 μM), 2OG (1 mM), L-ascorbate (1 mM), Fe(II) ammonium sulfate (80 μM), and 1 ml of 1 mg/ml TSP as an internal standard in ammonium formate buffer in D_2O (pD 7.9). The first acquisition was completed 15 min after addition. Spectra were acquired using 1D NOESY water pre-saturation (Bruker pulse program: *noesygppr1d*) using 16 (ALKBH5) or 32 (FTO) scans and a relaxation delay of 2 s. Control experiments' spectra (ssRNA and HCHO spiked in) were acquired for 160 scans. The temperature of the probe was 310 K for the reaction with FTO. For the reaction of ALKBH5, the temperature of the probe was 298 K for the first 25 min, and then 310 K for the remainder of the time course. NMR spectra were measured using a Bruker AVIII 700 MHz NMR spectrometer equipped with a TCI helium cooled cryoprobe. Data were processed with TopSpin v.3.5.6. The samples were prepared in 3-mm-diameter MATCH NMR tubes (Hilgenberg).

NMR monitoring of FTO and ALKBH5 on unlabelled m^6A nucleoside or 8-mer m^6A-containing ssRNA as substrate

Assay mixtures contained ALKBH5 (20 μM) or full-length FTO (10 μM); for reactions with ssRNA $UGGm^6AACUGC$ (800 μM), full-length FTO (20 μM) or ALKBH5 (20 μM) was used. For reactions in the absence of substrate, full-length FTO (20 μM) was used. m^6A nucleoside was purchased from Sigma–Aldrich and ssRNA $UGGm^6AACUGC$ was purchased from Dharmacon RNA synthesis. With the m^6A nucleoside potential substrate, reactions contained FTO or ALKBH5 (20 μM), 2OG (800 μM), Fe(II) ammonium sulfate (200 μM), m^6A nucleoside (800 μM), sodium L-ascorbate (1 mM), and an internal standard (TSP, 800 μM). For FTO reactions, 50 mM ammonium formate buffer in D_2O (pD 7.5) was used; for ALKBH5 reactions, 50 mM ammonium formate buffer in D_2O (pD 7.9) was used. For the reaction of FTO with ssRNA $UGGm^6AACUGC$, 2OG (5 mM) and Fe(II) ammonium sulfate (400 μM) were used. All other concentrations were the same.

NMR spectra were measured using a Bruker AVIII 700 MHz NMR spectrometer equipped with a TCI helium cooled cryoprobe. Data were processed with TopSpin v.3.6.2. 1D NOESY with pre-saturation (Bruker pulse program: *noesygppr1d*) using 64 scans and a relaxation delay of 2 s; data were treated with an exponential function with 2 Hz line broadening, prior to Fourier transformation, with the exception of the full-length FTO reaction without substrate where 0.3 Hz line broadening was applied, due to the low intensity of the succinate peak. Spectra were acquired every 5 min over 120 min. For the reaction of full-length FTO with ssRNA $UGGm^6ACUGC$, two additional time points were obtained, i.e. at ∼2880 min, before and after the addition of $H^{13}CHO$. One additional time point was acquired at ∼2880 min for the uncoupled reaction of full-length FTO in the absence of substrate. All spectra were recorded at 298 K. All samples were prepared in 3-mm-diameter MATCH NMR tubes (CortecNet).

Results

FTO catalyses internal m^6A hydroxylation and ALKBH5 catalyses m^6A demethylation in ssRNA

To compare the activities of recombinant FTO and ALKBH5, we initially produced the proteins in highly purified forms via reported procedures [48, 54–56]. For FTO, we used both full-length FTO and a truncated FTO construct ($FTO_{32–505}$, FTOΔ31); the truncated construct has been shown to have similar activity to full-length FTO [60]. We then analysed their reactions, using an 8-mer m^6A-containing ssRNA substrate (8-mer m^6A ssRNA) with m^6A at the fourth position ($UGGm^6ACUGC$) (Fig. 2). Incubations were carried out as reported in the presence of Fe(II), O_2, 2OG, and ascorbate at pH 7.2 or 7.5 [48, 49].

We initially monitored full-length FTO (0.5 and 0.25 μM)-catalysed substrate depletion and product formation (pH 7.5) over 45 min using ion-paired chromatography followed by negative ion electrospray ionization (ESI)-MS (IP-RP-LC/ESI-MS) using a XEVO G2-QTOF spectrometer with the same 8-mer m^6A RNA substrate (Supplementary Figs S1A and S2). The major observed product of FTO catalysis was hm^6A (1276.1832, corresponding to the −2 charge state), with the N^6-demethylated product comprising <5% of the total products; there was no evidence for f^6A formation. A low-level peak potentially corresponding to an N^6-methyleneadenosine/imine (or other tautomer) was also observed (1267.6827, −2). By contrast, analysis of $ALKBH5_{66–292}$ catalysis at various concentrations (8, 4, and 2 μM) using the same method showed that the major product was the N^6-demethylated species (m/z 1261.1696, −2), with only very low levels of a peak corresponding to hm^6A formation (1276.0139, −2) being observed, possibly reflecting reaction of HCHO produced by demethylation with the demethylated product (Supplementary Figs S1B and S3).

We then monitored FTOΔ31-catalysed substrate depletion and product formation at pH 7.2, that in the cell nucleus, over 45 min by direct injection into a SCIEX Triple TOF 6600 (QTOF) mass spectrometer, analysing in the negative ion mode (Fig. 2 and Supplementary Fig. S4). At early time points (<5 min), we observed a new peak corresponding to hm^6A (m/z 509.86, −5) and 8-mer m^6A ssRNA substrate (m/z 506.67, −5), with no evidence for N^6-demethylated 8-mer ssRNA (m/z 503.86, −5) (Fig. 2A and Supplementary Fig. S4). A peak corresponding to N^6-demethylated 8-mer ssRNA was first observed after 5 min; the intensity of this peak increased over the subsequent time course. Notably, at all the time points up to 45 min, hm^6A was the dominant observed product (Fig. 2B and Supplementary Fig. S4). Low levels of peaks potentially corresponding to f^6A (m/z 509.46, −5) and an imine

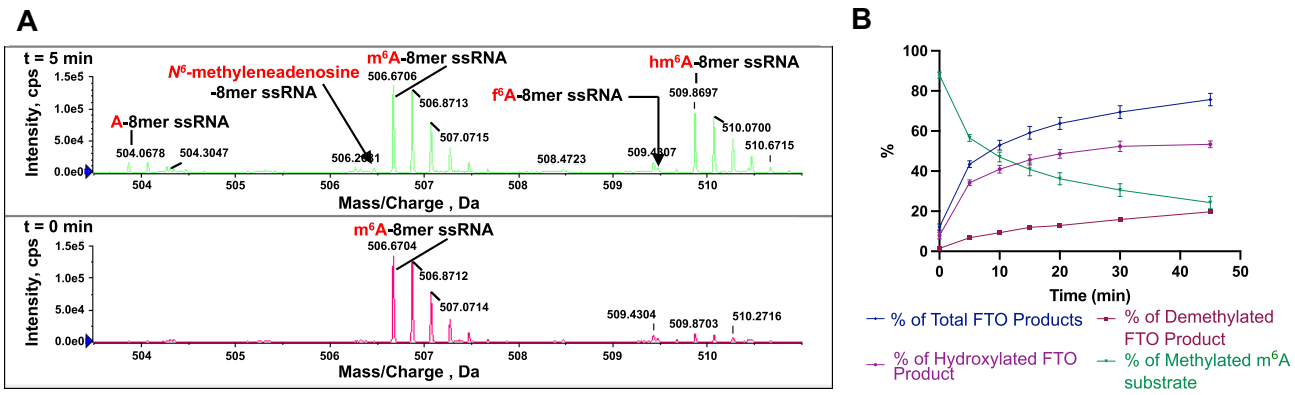

Figure 2. Evidence FTO acts as hydroxylase and ALKBH5 as a demethylase. (**A**) QTOF-MS time-course analysis of internal 8-mer m^{6}A ssRNA (UGGm^{6}ACUGC) by FTOΔ31. The extracted spectra at different time points indicate the 8-mer m^{6}A ssRNA (m/z 506.67, −5 charge state) is converted to a hydroxylated product (hm^{6}A) (m/z 509.86, −5), which was the major product throughout the time course (45 min). Peaks for the N^6-demethylated product (m/z 503.86, −5) increase as the reaction progresses, likely due to non-enzymatic fragmentation of hm^{6}A. Evidence for formation of f^{6}A (m/z 509.46, −5) and imine products (m/z 506.46, −5) (indicated by arrows) was not accrued under these conditions. (**B**) Plots showing the reaction product profile of internal 8-mer m^{6}A ssRNA oligo by FTOΔ31 at different time points (prepared using GraphPad Prism 10.1.1). Reactions were performed in triplicate ($n = 3$); error bars represent the standard error of the mean (SEM) (see also Supplementary Fig. S3).

(m/z 506.46, −5) were also observed over the course of the reaction, but the intensities of these peaks were insufficient to assign them as enzyme products; note that evidence for imine was not observed by ^{1}H NMR (see below) and it is possible that conversion of m^{6}A to the imine occurs in the mass spectrometer [49].

We then analysed the FTO and ALKBH5 reactions by ^{1}H NMR (700 MHz), initially at 25°C using an m^{6}A nucleoside substrate. Consistent with prior NMR studies [49], full-length FTO catalysed oxidation of the m^{6}A nucleoside to give the hm^{6}A product, as observed by appearance of a broad peak corresponding to a hemiaminal methylene at δ_H 5.1 ppm (Fig. 3). Clear evidence for conversion of 2OG to succinate was observed by ^{1}H NMR, but at a higher level than for conversion of m^{6}A to hm^{6}A, potentially reflecting substrate analogue promoted uncoupled 2OG turnover (Fig. 3 and Supplementary Figs S5 and S6). By contrast, there was no evidence for ALKBH5-catalysed oxidation of the m^{6}A nucleoside and only low levels of turnover of 2OG to succinate were observed (Supplementary Fig. S7), possibly reflecting uncoupled and/or non-enzymatic reaction [61, 62].

We then investigated FTO and ALKBH5 catalysis using selectively ^{13}C-methyl-labelled m^{6}A (^{13}C-m^{6}A); gradient-selected 1D heteronuclear single quantum correlation (^{1}H–^{13}C-HSQC) with $^1J_{CH}$ optimized to 145 Hz and ^{1}H NMR spectra were acquired (at 37°C). With FTO, 15 min after initial mixing (when the first acquisition was complete), the N^6-$^{13}CH_2OH$ group was observed at δ_H 5.04 ppm and δ_H 5.26 ppm ($^1J_{CH} = 160$ Hz). New resonances corresponding to anomeric (δ_H 6.07 ppm) and aromatic protons of ^{13}C-hm^{6}A (δ_H 8.33 ppm) were observed, but resonances corresponding to ^{13}C-labelled formaldehyde ($^{13}CH_2O$) were not observed (Fig. 4), suggesting that the observed product of FTO is hm^{6}A in the absence of fragmentation of the hemiaminal. The appearance of the N^6-$^{13}CH_2OH$ resonances correlated with succinate formation and inversely with reduction of the N^6-[^{13}C]-CH_3 resonances. Approximately 40 min after initial mixing, a peak at δ_H 4.92 ppm was observed, indicating the formation of H^{13}CHO; the increase in the $^{13}CH_2OH$ resonance correlated inversely with a decrease in the N^6 H^{13}CHO resonances (Fig. 4). The presence of H^{13}CHO was confirmed by spiking with authentic H^{13}CHO (Fig. 4). The formation of succinate was observed to halt ∼40 min after the reaction had been started (possibly due to the limited availability of oxygen); however, the H^{13}CHO resonances continued to increase even after 600 min after initial mixing (Fig. 4). This observation indicates that the formation of H^{13}CHO is, at least partially, a non-enzyme-catalysed process, likely involving gradual hm^{6}A fragmentation. We measured the Michaelis–Menten constant, K_M, of m^{6}A nucleoside as a substrate of FTO by HPLC and found that it was 791 μM (Supplementary Fig. S8), a relatively high value, suggesting that m^{6}A in the nucleoside form is likely not a physiologically relevant substrate in cells. Despite use of various conditions (e.g. varied temperature, ionic strength), ALKBH5 was not observed to catalyse effective oxidation of the ^{13}C-m^{6}A nucleoside.

We next investigated FTO and ALKBH5 catalysis using a 5-mer ssRNA-containing m^{6}A (GGm^{6}ACU) as a substrate in the presence of 2OG, ascorbate, and ferrous iron in ammonium formate buffer in D_2O at pD 7.9. With FTO, 15 min after mixing (when the first ^{1}H NMR acquisition was complete), a broad resonance at δ_H 5.1 ppm, corresponding to the hemiaminal methylene of GGhm^{6}ACU, was observed. New resonances corresponding to the aromatic protons of GGhm^{6}ACU at δ_H 7.68 ppm (C), δ_H 7.8 ppm (U), and δ_H 8.24 ppm (hm^{6}A) and overlapping resonances at δ_H 7.88 ppm (G) and δ_H 7.94 ppm (G) were observed (Fig. 5). A quantifiable formaldehyde resonance at δ_H 4.88 ppm was not observed until 1 h after mixing.

For ALKBH5, the initial acquisition was done at 298 K (25 min) to slow catalysis and potentially enable hm^{6}A detection; however, with the exception of succinate, new resonances were not observed (Supplementary Fig. S9). The temperature was then increased to 310 K (6 min), and a peak at δ_H 4.83 ppm corresponding to hydrated formaldehyde was observed after completion of the first acquisition (Supplementary Fig. S9), along with resonances corresponding to anomeric and aromatic protons of (demethylated) GGACU. Peaks corresponding to the hemiaminal methylene of GGhm^{6}ACU were not observed throughout the ALKBH5-catalysed reactions,

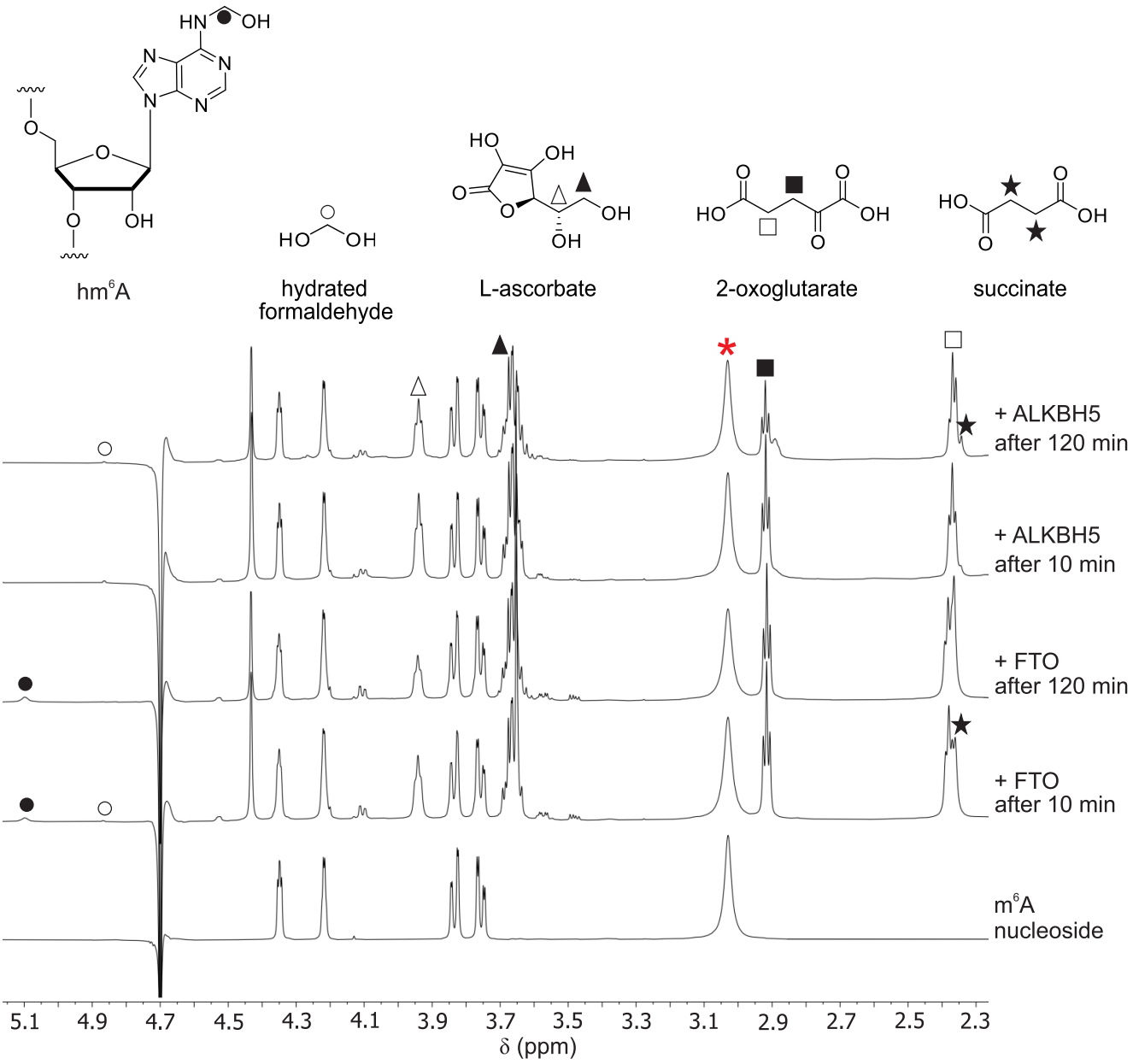

Figure 3. NMR evidence that FTO is a hydroxylase using m^{6}A nucleoside as a substrate, while ALKBH5 is unable to efficiently catalyse m^{6}A nucleoside oxidation. ^{1}H NMR time-course spectra (700 MHz) of m^{6}A nucleoside oxidation as catalysed by full-length FTO and potential m^{6}A nucleoside oxidation by ALKBH5 are shown. FTO mediated oxidation is observed after 120 min as evidenced by a decrease in peak area of the broad resonance at δ_H 3.02 ppm (red asterisk) corresponding to m^{6}A N^6-CH_3; this resonance was unchanged with ALKBH5. The peak at δ_H 5.10 ppm (black circle) corresponding to hm^{6}A hemiaminal increased with FTO; no evidence for the hemiaminal was observed with ALKBH5. With FTO, there was a decrease in the 2OG methylene peaks (δ_H 2.93 ppm, black squares; 2.37 ppm, open squares) correlating with an increase in the succinate peak (δ_H 2.34 ppm, black star). With ALKBH5 there was only a slight decrease in the 2OG peak and a slight increase in the succinate peaks indicating substrate uncoupled or non-enzymatic oxidation of 2OG. Low levels of hydrated formaldehyde (δ_H 4.87 ppm, open circles) were observed with FTO and ALKBH5, likely substantially derived from the ammonium formate buffer.

supporting ALKBH5-catalysed demethylation of m^{6}A in ssRNA.

We also investigated FTO and ALKBH5 catalysis by NMR at 25°C using an 8-mer ssRNA-containing m^{6}A as substrate. We observed production of hm^{6}A by FTO, while there was no evidence of hm^{6}A production by ALKBH5 (Supplementary Figs S10 and S11), consistent with our results using 5-mer ssRNA.

We investigated whether ALKBH5$_{66–292}$ can catalyse fragmentation of hm^{6}A in an 8-mer ssRNA, prepared using FTO, using the IP-RP-LC/ESI-MS method (Supplementary Fig. S12A). After production of hm^{6}A, FTO was removed and ALKBH5 was added to the solution. We observed levels of the demethylated product (1261.1766, −2) increased (due to ALKBH5 catalysis), while the hm^{6}A (m/z 1276.1832, −2) levels remained relatively constant. After 15 min, a very low level peak corresponding to a new product, potentially f^{6}A (m/z 1274.9894, −2) was observed (Supplementary Fig. S12B). These observations imply ALKBH5 does not efficiently catalyse fragmentation of hm^{6}A in solution, at least under the

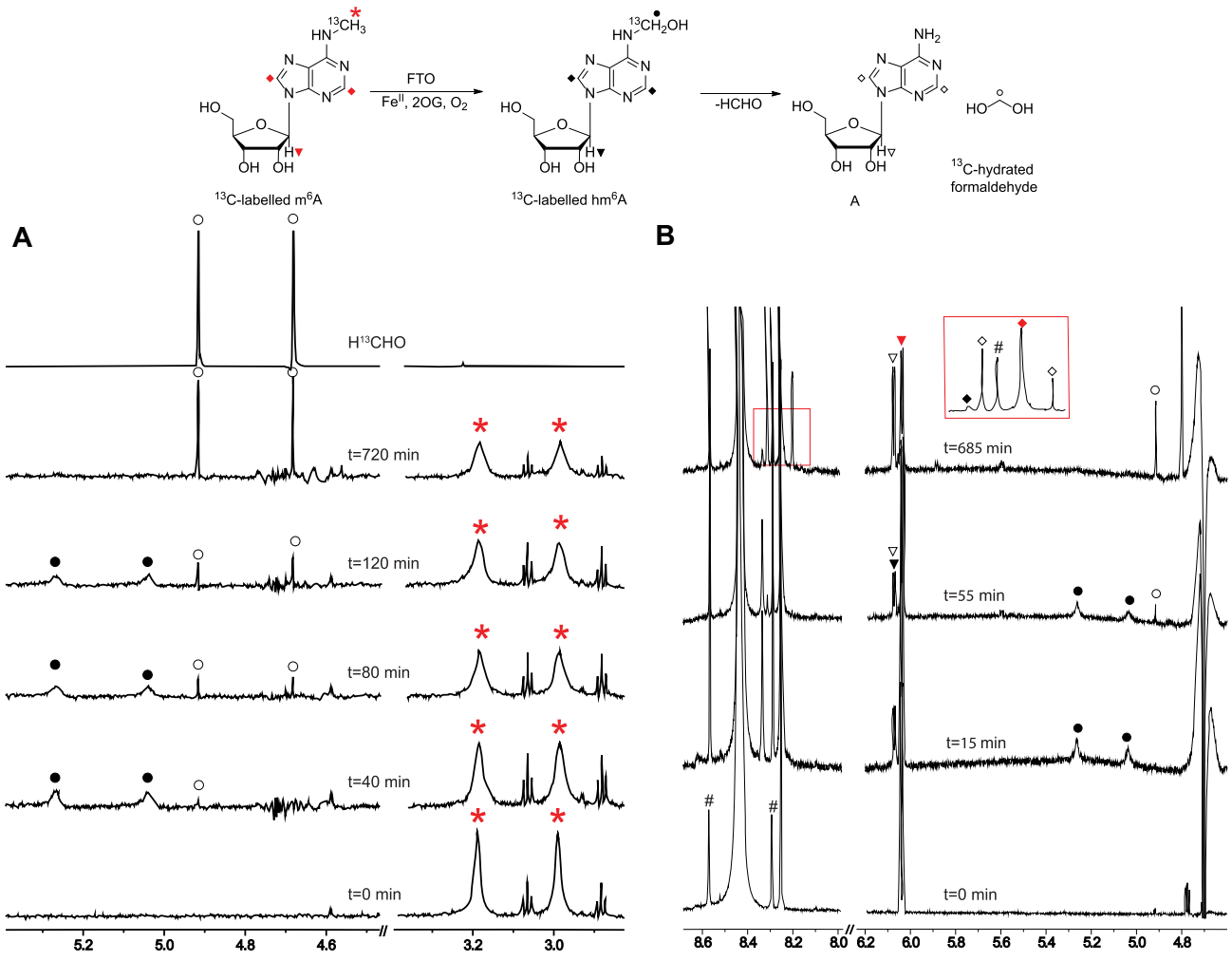

Figure 4. FTO-catalysed ^{13}C-m^{6}A NMR time course at 310 K. ^{1}H resonances bonded to a [^{13}C]-carbon appear as doublets due to the $^1J_{CH}$ coupling. Alternating (**A**) 1D HSQC and (**B**) ^{1}H NMR time-course spectra of FTO-catalysed oxidation with ^{13}C-m^{6}A. Assigned resonances: (i) δ_H 2.99 ppm and δ_H 3.19 ppm, ^{13}C-labelled methyl m^{6}A (red asterisks); (ii) δ_H 4.68 ppm and δ_H 4.92 ppm, hydrated ^{13}C-formaldehyde (open circles); (iii) δ_H 5.03 ppm and δ_H 5.26 ppm, hemiaminal (N-^{13}CH$_2$OH, solid circles); (iv) δ_H 6.03 ppm (m^{6}A, inverted red triangle) and δ_H 6.07 ppm (hm^{6}A, inverted black solid triangle and A, inverted black triangle), anomeric protons; and (v) δ_H 8.25 ppm (m^{6}A, red rhombus), δ_H 8.33 ppm (hm^{6}A, black solid rhombus), and δ_H 8.20 ppm and δ_H 8.31 ppm (A, open rhombus), aromatic protons. Satellite resonances of buffer: #.

tested conditions. Note this conclusion does not argue against a protein-bound hm^{6}A intermediate during ALKBH5 catalysis, since 2OG oxygenase catalysis (normally) proceeds via a multi-step ordered sequential mechanism [34, 35].

To confirm that ALKBH5 possesses hm^{6}A fragmentation activity, we performed QTOF-MS time-course assays on the catalysis of 8-mer m^{6}A ssRNA oxidation by ALKBH5$_{74–292}$ wild-type construct and the ALKBH5$_{74–292}$ K132E mutant, in which a critical lysine involved in hm^{6}A fragmentation had been mutated, in the presence and absence of inhibitor pydridine-2,4-dicarboxylate (2,4-PDCA), an ALKBH5 inhibitor [33, 55, 56] (Supplementary Figs S13–S16). For the ALKBH5$_{74–292}$ wild-type construct, regardless of the presence of 2,4-PDCA, an increase in demethylated product (m/z 503.86, −5) but not hm^{6}A ssRNA (m/z 509.86, −5) was observed (Supplementary Figs S13 and S14). While 2,4-PDCA appeared to reduce the activity of wild-type ALKBH5$_{74–292}$, it did not result in accumulation of hm^{6}A (Supplementary Fig. S14), suggesting that the absence of hm^{6}A is not the result of the high activity of recombinant ALKBH5$_{74–292}$. On the other hand, the ALKBH5$_{74–292}$ K132E mutant, both in the presence and in the absence of 2,4-PDCA, produced hm^{6}A (m/z 509.86, −5) (Supplementary Figs S15 and S16). These results suggest that ALKBH5 is a *bona fide* demethylase that is dependent on Lys132 for its hm^{6}A fragmentation activity.

The combined MS and NMR results imply that the catalytic activity of FTO results in m^{6}A hydroxylation giving hm^{6}A. Although we cannot rule out the possibility that some demethylated product is directly produced at the FTO active site, our results imply most, if not all, of the observed demethylated product observed during FTO catalysis is produced with an observable time delay post-hydroxylation by FTO, likely as a result of non-enzymatic fragmentation of hm^{6}A. By contrast with FTO, ALKBH5 is an efficient m^{6}A demethylase. Note that although hm^{6}A is relatively stable from a kinetic perspective, it is not thermodynamically stable and an excess of HCHO is required to observe substantial formation of hm^{6}A under equilibrating conditions, as observed in reported NMR studies [49].

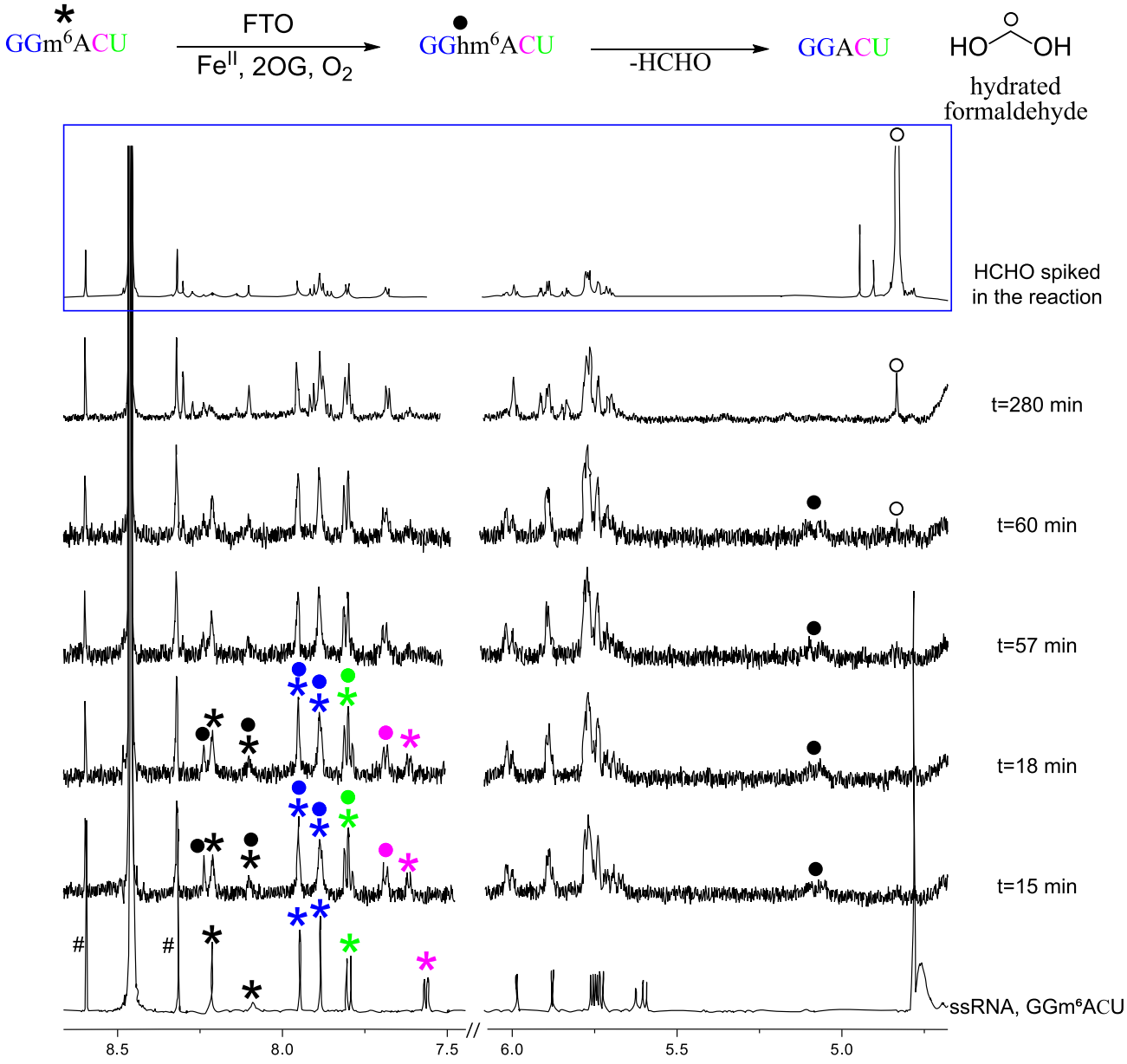

Figure 5. FTO-catalysed ssRNA GGm^{6}ACU NMR time course. ^{1}H NMR (310 K) time course showing FTO-catalysed hemiaminal (m^{6}A) formation. Conditions: FTO (20 μM), 2OG (1 mM), sodium-L-ascorbate (1 mM), Fe(II) ammonium sulfate (80 μM), and GGm^{6}ACU (200 μM) in ammonium formate buffer in D_2O (pD 7.9). The first acquisition (32 scans) was completed 15 min after mixing. The evidence for hemiaminal methylene peak (hm^{6}A; black solid circle) was observed as a broad peak at δ_H 5.1 ppm; hm^{6}A slowly fragments into adenosine and formaldehyde (δ_H 4.88 ppm; black open circle). *In situ* generated formaldehyde resonances matched with the authentic HCHO spiked into the reaction. Aromatic resonances corresponding to nucleosides in GGm^{6}ACU (asterisk) appear at (i) δ_H 7.56 ppm (C, pink), (ii) δ_H 7.80 ppm (U, green), (iii) δ_H 7.88 ppm and δ_H 7.94 ppm (G, blue), and (iv) δ_H 8.09 ppm and δ_H 8.21 ppm (m^{6}A, black); and GGhm^{6}ACU (solid circle) appear at (i) δ_H 7.68 ppm (C, pink), (ii) δ_H 7.80 ppm (U, green), (iii) δ_H 7.88 ppm and δ_H 7.94 ppm (G, blue), and (iv) δ_H 8.24 ppm (hm^{6}A, black). Satellite resonances of ammonium formate buffer: #. Control experiments', first (ssRNA) and last (HCHO spiked), spectra consisted of 160 scans.

FTO catalyses oxidation of a 5′-cap mRNA substrate producing hm^{6}A$_m$

There is evidence that the reaction outcomes of some 2OG oxygenases are affected by context, e.g. substrate length or conformation with polymeric substrates [31, 63]. We were thus interested to study the FTO reaction products, in particular with respect to whether hydroxylation or demethylation occurs, with m^{6}A$_m$, a reported FTO substrate adjacent to the 5′ N^7-methylguanosine (m^{7}G) cap [27, 28]. To investigate this, we tested 6-mer m^{7}Gpppm^{6}A$_m$ ssRNA (m^{7}Gpppm^{6}A$_m$UACUU) as a substrate of FTOΔ31 and ALKBH5$_{74–292}$, with incubation conditions as before analysing by SCIEX Triple TOF 6600 (QTOF) mass spectrometer. As reported [27, 28], ALKBH5$_{74–292}$ was not observed to catalyse oxidation of m^{7}Gpppm^{6}A$_m$ ssRNA (Supplementary Fig. S17). Consistent with the studies of full-length FTO and FTOΔ31 with the 8-mer m^{6}A ssRNA substrate, with FTOΔ31 and m^{7}Gpppm^{6}A$_m$UACUU, the hm^{6}A$_m$ product

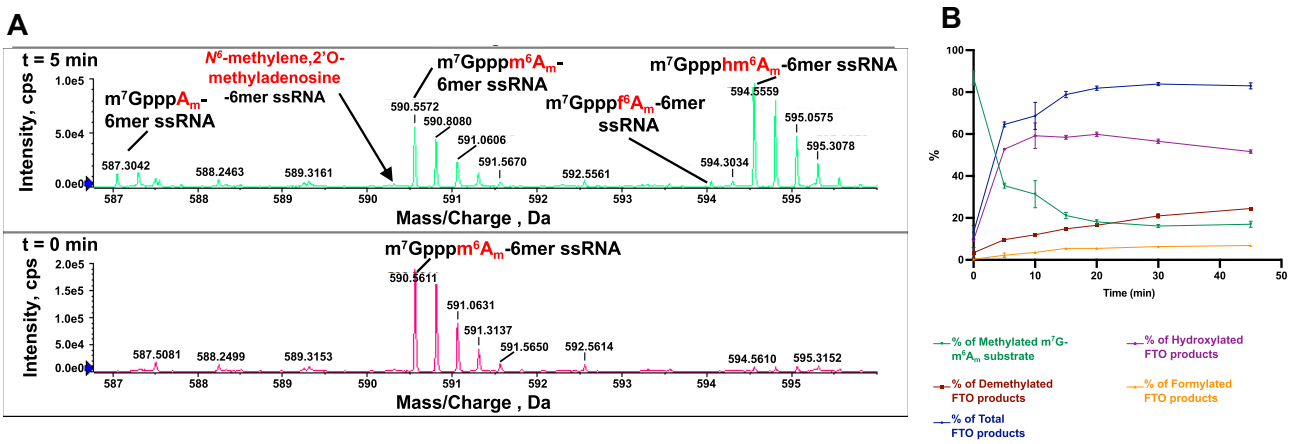

Figure 6. FTO-catalysed oxidation of a 5′-cap substrate. (**A**) QTOF-MS time-course analysis of 6-mer $m^7Gpppm^6A_m$ ssRNA ($m^7Gpppm^6A_mUACUU$) oxidation as catalyed by FTOΔ31. The extracted spectra recorded at different time points indicate 6-mer $m^7Gpppm^6A_m$ ssRNA oligo (*m/z* 590.56, −4) is converted to a hm^6A_m product (*m/z* 594.56, −4), which was the major observed product throughout the time course (45 min). Peaks for the demethylated product (*m/z* 587.06, −4) intensify as the reaction progresses. Evidence for a second apparent oxidation product, f^6A_m (*m/z* 594.06, −4), was also observed, albeit at low levels. Similarly to reaction of FTO with the 8-mer m^6A ssRNA, evidence for an imine species (*m/z* 590.31, −4) was not detected (as indicated by arrows). (**B**) Plots showing the reaction product profile for FTOΔ31-catalysed oxidation of 6-mer $m^7Gpppm^6A_m$ ssRNA, (generated using GraphPad Prism 10.1.1). Reactions were performed in triplicate ($n = 3$); error bars represent the standard error of the mean (SEM).

(*m/z* 594.56, −4) dominated at all time points (Fig. 6A and B, and Supplementary S18). By contrast with hm^6A_m, levels for which decreased after 20 min, masses corresponding to the demethylated (A_m) (*m/z* 587.06, −4) and (apparent) formylated (f^6A_m) products (*m/z* 594.06, −4) increased over time (Fig. 6B), though internal f^6A was only observed at low levels (Fig. 2A). These observations suggest that FTO could produce a relatively stable hm^6A_m by the 5′ cap of RNA, the potential biological roles of which require further investigation.

Non-enzyme-catalysed fragmentation of FTO products

We then carried out experiments to investigate whether the relatively low levels of N^6-demethylated 8-mer ssRNA and demethylated $m^7Gpppm^6A_mUACUU$ produced in FTO reactions are due to enzyme- or non-enzyme-mediated reactions. Thus, FTOΔ31 was incubated with 8-mer internal m^6A ssRNA and $m^7Gpppm^6A_mUACUU$ separately for 30 min as previously described. 2,4-PDCA, a known FTO inhibitor [55], or a control solution was then added and the reactions were analysed by QTOF-MS as before. In both the 2,4-PDCA and control treated samples, the hm^6A levels were similar at the same time points (Fig. 7A and B). The demethylated product levels manifested an increase over time, consistent with studies on hm^6A stability [49] and its non-enzyme-catalysed fragmentation with or without FTO. We examined the kinetics of hm^6A fragmentation at pH 7.2 (pH in the nucleus), observing first-order kinetics with similar decay constants in the presence (3.9×10^{-3} min^{-1}) and absence (3.2×10^{-3} min^{-1}) of 2,4-PDCA. Under these conditions, the half-lives of hm^6A with and without 2,4-PDCA were calculated as 176 and 211 min, respectively (Fig. 7C).

We studied the fragmentation of FTOΔ31 generated 5′ m^7G triphosphate hm^6A_m cap into A_m by adding 2,4-PDCA or a control solution after 10 min incubation, a time when hm^6A_m product levels were maximal (Fig. 7D and E). Both the 2,4-PDCA-treated and non-PDCA-treated samples manifested similar first-order decay rates for the hm^6A_m product, with decay constants/half-lives of 5.4×10^{-3} min^{-1}/128 min and 5.0×10^{-3} min^{-1}/138 min, respectively, under these conditions (Fig. 7F). As before, these observations imply that hm^6A_m fragmentation is, at least predominantly, not FTO-catalysed, supporting the proposal that FTO acts as a hydroxylase within the context of m^6A_m oxidation adjacent to the 5′ cap.

AlkB, ALKBH2, and ALKBH3 do not act as m^1A hydroxylases

To investigate whether the hydroxylase activity of FTO is unusual, we carried out studies with DNA damage repair 2OG oxygenases (Fig. 1D), i.e. human ALKBH2 and ALKBH3 and their bacterial homologue AlkB using 1mA ssDNAs as substrates, with analysis by ion-paired ESI-MS (Supplementary Figs S19–S21). Note that some reported ALKBH2/3 and AlkB studies have used substrate digestion and monitoring through LC or MS [40, 43], a method that can result in the loss of hemiaminal detection. The products of undigested ALKBH2/3 and AlkBΔN11 reactions were analysed by IP-RP-LC/ESI-MS. We observed evidence for demethylated adenosine without evidence for N^1-hydroxymethyldeoxyadenosine (1hmA), N^1-formyldeoxyadenosine, or imine products in all three cases (Supplementary Figs S19–S21). Thus, ALKBH2/3 and AlkB converted an m^1A-containing ssDNA substrate to the demethylated products; note these observations are consistent with knowledge that 1hmA is relatively less stable compared to 6hmA [49].

Discussion

The MS and NMR assay results presented here support previous studies showing both FTO and ALKBH5 act on internally located m^6A in ssRNA [14, 15]. In accord with prior studies, FTO, but not ALKBH5, catalyses oxidation of $m^7Gpppm^6A_m$ ssRNA [27, 28] (Fig. 6 and Supplementary Fig. S18). However, whereas with ALKBH5 the only observed product with m^6A (8-mer m^6A ssRNA) was the demethylated adenosine (Supplementary Figs S1B and S13),

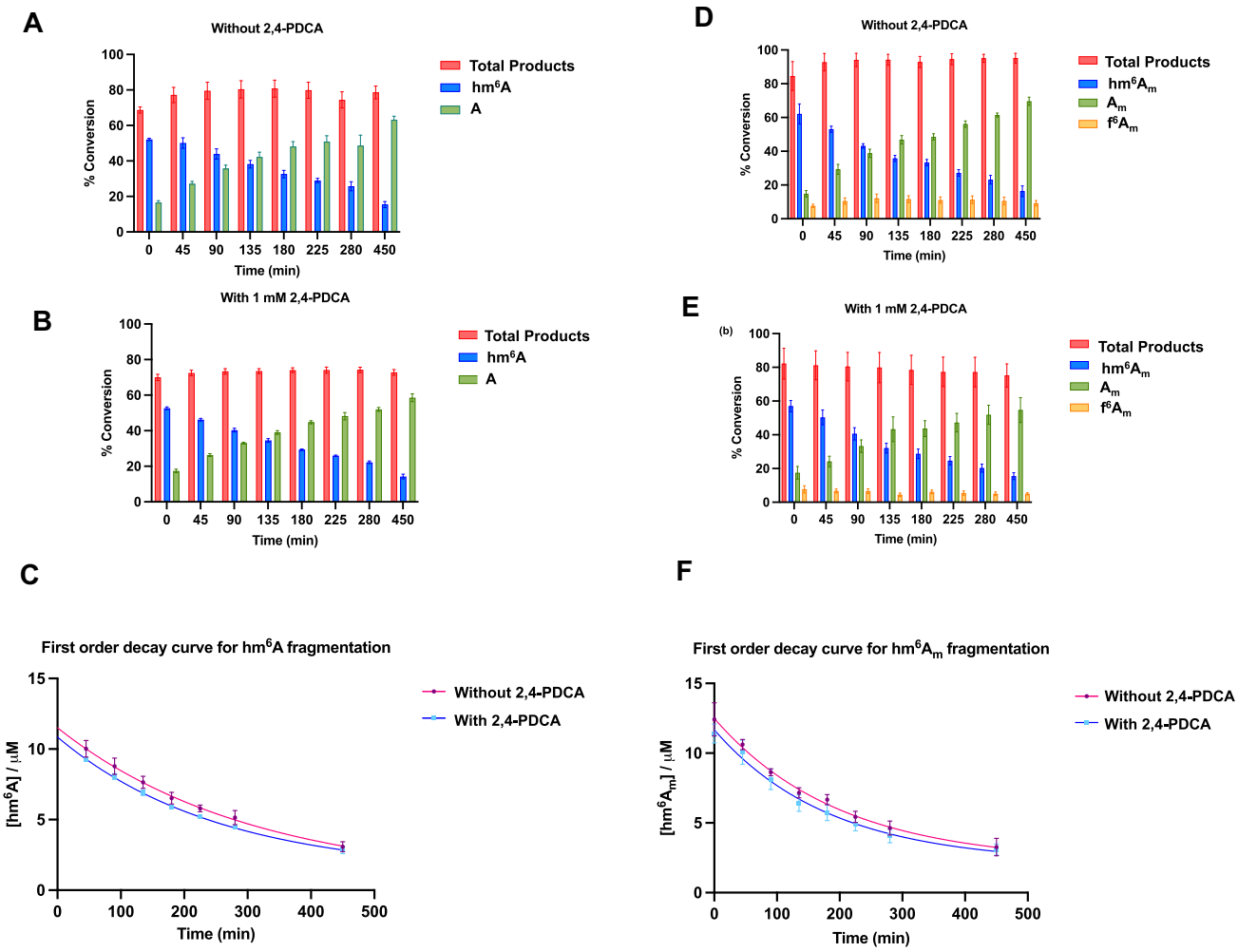

Figure 7. Non-enzymatic fragmentation of hm^6A/hm^6A_m produced by FTO catalysis. FTOΔ31-catalysed oxidation of 8-mer m^6A ssRNA oligo (UGGm^6ACUGC) for 30 min results in ∼50% conversion to hm^6A. FTO products were monitored over 450 min by QTOF-MS: (**A**) without 2,4-PDCA and (**B**) with 1 mM 2,4-PDCA. Bar graphs (generated using GraphPad Prism 10.1.1) show the presence of 2,4-PDCA does not substantially affect the rate of hm^6A fragmentation to N^6-demethylated 8-mer ssRNA, indicating that hm^6A fragmentation is, at least mostly, not enzyme catalysed. Error bars represent SEM of duplicates ($n = 3$). (**C**) [hm^6A] versus time plot for first-order kinetics of hm^6A degradation, with and without 2,4-PDCA (generated using GraphPad Prism 10.1.1). Data were fitted into a one-phase decay model. Error bars represent SEM ($n = 3$). Both reactions show similar trends for non-enzymatic fragmentation of hm^6A and follow first-order kinetics with similar decay rate constants. After initial hydroxylation of 6-mer $m^7Gpppm^6A_m$ ssRNA ($m^7Gpppm^6A_m$UACUU) as catalysed by FTOΔ31 (∼50% hm^6A_m generated after 10 min), the sample was divided into two portions and treated with the FTO inhibitor 2,4-PDCA (**E**) or a buffer control (**D**). Products were monitored by QTOF-MS over 450 min. Both reactions show similar profiles, implying that hm^6A_m fragmentation is not enzyme mediated. (**F**) [hm^6A_m] versus time plots for first-order kinetics of hm^6A_m fragmentation with and without the addition of 2,4-PDCA. Data were fitted with a one-phase decay model; curves were generated using GraphPad Prism 10.1.1. Reactions were performed in triplicate ($n = 3$); error bars represent the SEM. The fragmentation of hm^6A_m adheres to first-order decay kinetics and exhibits comparable decay profiles with or without 2,4-PDCA, implying that FTO does not catalyse hm^6A fragmentation.

with FTO both substrate types produced a hemiaminal (hm^6A/hm^6A_m) species as the dominant product at all time points (Figs 2–6 and Supplementary Figs S1, S2, S4, and S18). Both the NMR and MS evidence showed that at early time points, FTO produces a hemiaminal species as the only observed product, without the presence of a demethylated product. Support for the unusual nature of FTO catalysis comes from studies with human ALKBH2 and ALKBH3 and bacterial AlkB, which manifested demethylation reactions with m^1A-containing substrates (Supplementary Figs S19–S21). Our results also showed that while FTO can act on m^6A nucleoside, ALKBH5 did not show activity against m^6A nucleoside. Kinetic studies of FTO on m^6A nucleoside showed that its K_M is 791 μM, a level much higher than expected for m^6A nucleosides in cells [64, 65], suggesting that FTO likely does not function in oxidizing N^6-methyl of m^6A nucleosides in cells.

The results of studies where FTO reactions with internal m^6A or $m^7Gpppm^6A_m$ substrates were halted by the addition of an inhibitor [55] imply that the slow fragmentation of FTO-produced hm^6A/hm^6A_m giving the demethylated product and formaldehyde that is observed in the presence of FTO is not enzyme catalysed (Fig. 7A–F). ALKBH5 did not catalyse fragmentation of hm^6A produced by FTO catalysis in solution (Supplementary Fig. S12). This could be because ALKBH5 prefers binding to m^6A-containing ssRNA more so than the hm^6A-containing ssRNA. Note, however, that the normally ordered sequential nature of 2OG oxygenase catalysis means protein-bound hm^6A may be a protein-

bound intermediate during ALKBH5 catalysis. Our observations are consistent with prior studies demonstrating the enhanced stability of exocyclic N-linked hemiaminals compared to endocyclic nitrogens, though the latter are faster to form in reactions with formaldehyde [49, 51]. Catalysis by a mutant ALKBH5 K132E demonstrated that the N-linked hemiaminal can be detected by MS, indicating that wild-type ALKBH5 is a *bona fide* m^6A demethylase.

The combined results strongly indicate that FTO acts as a hydroxylase, initially at least, producing hemiaminal-type products. Further work is required to validate reports that FTO-catalysed reactions on $m^7Gpppm^6A_m$-containing ssRNA can produce low levels of f^6A_m [32, 33, 48, 49], likely produced by hm^6A_m oxidation (Fig. 6 and Supplementary Fig. S18). Note that the low levels of f^6A_m produced mean that as yet we have been unable to validate its proposed structure by NMR. Further, clear evidence for the formylated f^6A product was not apparent with the ssRNA internal m^6A substrate (Fig. 2 and Supplementary Figs S1 and S4). In some MS analyses, there was also evidence for N^6-methyleneadenosine/imine production [32], though it is uncertain whether this is a result of enzyme catalysis and/or due to dehydration from hm^6A/hm^6A_m under the MS analytical conditions; we did not see evidence for imine formation by NMR, though this could be because it was not present in sufficiently high levels.

If the formation of f^6A/f^6A_m can be validated in cells, FTO will be one of the set of 2OG oxygenases catalysing sequential oxidations on the same methyl group-derived carbon. Such activities were observed in early studies on 2OG oxygenases involved in gibberellin and cephalosporin biosynthesis [31, 66–68] and have been more recently observed in the ten-eleven translocation enzyme (TET)-mediated oxidation of 5-methylcytosine (5mC) in DNA, where sequential oxidations of a methyl group to an alcohol, then aldehyde, and then acid are observed (Fig. 1E) [69, 70]. Given that we observed evidence for low levels of f^6A, it is of interest that studies on the TET enzymes report that conversion of 5hmC to 5fC is slow compared to the initial oxidation of 5mC to 5hmC [32].

Most biological studies on FTO and ALKBH5 have focused on their roles as demethylases, affecting function (e.g. to modulate mRNA stability) by removal of m^6A methyl groups [15, 27, 30, 71–73]. Such roles are difficult to dissect, because they likely also involve m^6A methyltransferases and m^6A binding proteins [74]. One possibility is that the reactive products, including formaldehyde and hm^6A, produced by FTO-catalysed oxidations have functional roles, e.g. to enable cross-linking reactions with nucleic acids, proteins, or small molecules, as well precedented in hemiaminal/Schiff base (bio)chemistry [32, 49]. Although the FTO-catalysed production of hm^6A/hm^6A_m is striking, in a localized context, HCHO produced by ALKBH5 also has potential to enable similar reactions. Recent work has also shown that f^6A has potential to transfer a formyl group or undergo hydrolysis to produce formate [75]. Another possibility is that the transient reversible reaction of nucleophilic sites on proteins/nucleic acids with aldehydes serves to hinder irreversible/less reversible reactions, e.g. regulatory N-methylation or damaging alkylation [76]. It should also be noted that there is evidence that, at least in some cases, the substrate and product selectivities of 2OG oxygenases can vary with context, meaning the observations with isolated enzymes may not reflect *in vivo* activities [77], where other factors may alter substrate and product selectivities.

The combined results demonstrate a clear difference in the product selectivities of FTO and ALKBH5, at least in the case of studies with the isolated enzymes. How our biochemical observations relate to the proposed roles for FTO and ALKBH5 in healthy biology and disease is presently unclear. Among multiple reports, both FTO and ALKBH5 are linked to cancer, FTO is linked to obesity [16, 23], and ALKBH5 is linked to regulation of the hypoxic response and is a hypoxia-inducible factor target gene, i.e. is upregulated in hypoxia [78]. A recent study reports increased levels of cerebral formaldehyde in mice after acute high-altitude hypoxia exposure [78–80]. Mutations/variations in the *FTO*, but not the *ALKBH5*, gene are linked to diabetes and obesity [16, 23, 81], and it is possible that the different product selectivities of the two oxygenases reflect their different biological roles in disease. Given the role of aldehyde chemistry in diabetes [76], the ability of FTO to form hm^6A is of particular interest in this regard and is the subject of ongoing research. There are also reports linking FTO to aldehydes and alcohol consumption [82]. Further molecular investigations on the potential roles of ALKBH5, FTO, and other formaldehyde/hemiaminal producing oxygenases in the context of the physiological hypoxic response are thus of interest.

Acknowledgements

We thank Anthony Tumber, Shanrui Li, and Sylvia Mo for assistance in sample preparation and mass spectrometry data acquisition.

Author contributions: Simranjeet Kaur (Formal analysis [lead], Investigation [lead], Methodology [lead], Validation [lead], Visualization [lead], Writing—original draft [equal], Writing—review & editing [equal]), Pratheesh Maheswaran (Formal analysis [lead], Investigation [lead], Methodology [lead], Validation [lead], Visualization [lead], Writing—original draft [equal], Writing—review & editing [equal]), Samanpreet Kaur (Formal analysis [equal], Investigation [equal], Methodology [equal], Visualization [equal], Writing—original draft [equal], Writing—review & editing [equal]), Yingqi Lai (Formal analysis [equal], Investigation [equal], Methodology [equal], Visualization [equal]), Eidarus Salah (Methodology [supporting]), Dong Zhang (Investigation [supporting], Methodology [supporting]), Shifali Shishodia (Formal analysis [lead], Investigation [lead], Methodology [lead], Visualization [equal], Writing—original draft [equal], Writing—review & editing [lead]), Christopher J. Schofield (Conceptualization [lead], Funding acquisition [lead], Resources [lead], Supervision [lead], Writing—original draft [lead], Writing—review & editing [lead]), and Wei Shen Aik (Conceptualization [lead], Funding acquisition [lead], Resources [lead], Supervision [lead], Writing—original draft [lead], Writing—review & editing [lead])

Supplementary data

Supplementary data is available at NAR online.

Conflict of interest

None declared.

Funding

W.S.A. thanks the Research Grants Council, University Grants Committee, Hong Kong (General Research Fund 2022/23 [12302622]) for funding. W.S.A. thanks Hong Kong Baptist University for the Strategic Development Fund (SDFI8-1015-AOI) for equipment funding (SCIEX Triple TOF 6600 mass spectrometer). C.J.S. thanks Cancer Research UK (C8717/A18245) and the Biotechnology and Biological Sciences Research Council (BB/L009846/1) for funding. Research by the C.J.S. group was funded in part by the Wellcome Trust (106244/Z/14/Z). Funding to pay the Open Access publication charges for this article was provided by the University of Oxford.

Data availability

All data relevant to the results are included within the manuscript. MS and NMR data are available upon request.

References

1. Roundtree IA, Evans ME, Pan T *et al.* Dynamic RNA modifications in gene expression regulation. *Cell* 2017;**169**:1187–200. https://doi.org/10.1016/j.cell.2017.05.045
2. Shi H, Wei J, He C. Where, when, and how: context-dependent functions of RNA methylation writers, readers, and erasers. *Mol Cell* 2019;**74**:640–50. https://doi.org/10.1016/j.molcel.2019.04.025
3. Wei C-M, Gershowitz A, Moss B. N^6, $O^{2'}$-Dimethyladenosine a novel methylated ribonucleoside next to the 5′ terminal of animal cell and virus mRNAs. *Nature* 1975;**257**:251–3. https://doi.org/10.1038/257251a0
4. Keith JM, Ensinger MJ, Moss B. HeLa cell RNA (2′-O-methyladenosine-N^6-)-methyltransferase specific for the capped 5′-end of messenger RNA. *J Biol Chem* 1978;**253**:5033–9. https://doi.org/10.1016/S0021-9258(17)34652-5
5. Yang Y, Hsu PJ, Chen YS *et al.* Dynamic transcriptomic m^6A decoration: writers, erasers, readers and functions in RNA metabolism. *Cell Res* 2018;**28**:616–24. https://doi.org/10.1038/s41422-018-0040-8
6. Meyer KD, Saletore Y, Zumbo P *et al.* Comprehensive analysis of mRNA methylation reveals enrichment in 3′ UTRs and near stop codons. *Cell* 2012;**149**:1635–46. https://doi.org/10.1016/j.cell.2012.05.003
7. Dominissini D, Moshitch-Moshkovitz S, Schwartz S *et al.* Topology of the human and mouse m^6A RNA methylomes revealed by m^6A-seq. *Nature* 2012;**485**:201–6. https://doi.org/10.1038/nature11112
8. Ramanathan A, Robb GB, Chan SH. mRNA capping: biological functions and applications. *Nucleic Acids Res* 2016;**44**:7511–26. https://doi.org/10.1093/nar/gkw551
9. Wei C, Gershowitz A, Moss B. N^6, $O^{2'}$-Dimethyladenosine a novel methylated ribonucleoside next to the 5' terminal of animal cell and virus mRNAs. *Nature* 1975;**257**:251–3. https://doi.org/10.1038/257251a0
10. Tsukada Y-i, Fang J, Erdjument-Bromage H *et al.* Histone demethylation by a family of JmjC domain-containing proteins. *Nature* 2006;**439**:811–6. https://doi.org/10.1038/nature04433
11. Shi Y, Lan F, Matson C *et al.* Histone demethylation mediated by the nuclear amine oxidase homolog LSD1. *Cell* 2004;**119**:941–53. https://doi.org/10.1016/j.cell.2004.12.012
12. Shi Y. Histone lysine demethylases: emerging roles in development, physiology and disease. *Nat Rev Genet* 2007;**8**:829–33. https://doi.org/10.1038/nrg2218
13. Klose RJ, Kallin EM, Zhang Y. JmjC-domain-containing proteins and histone demethylation. *Nat Rev Genet* 2006;**7**:715–27. https://doi.org/10.1038/nrg1945
14. Jia G, Fu Y, Zhao X *et al.* N^6-Methyladenosine in nuclear RNA is a major substrate of the obesity-associated FTO. *Nat Chem Biol* 2011;**7**:885–7. https://doi.org/10.1038/nchembio.687
15. Zheng G, Dahl JA, Niu Y *et al.* ALKBH5 is a mammalian RNA demethylase that impacts RNA metabolism and mouse fertility. *Mol Cell* 2013;**49**:18–29. https://doi.org/10.1016/j.molcel.2012.10.015
16. Gerken T, Girard CA, Tung YC *et al.* The obesity-associated FTO gene encodes a 2-oxoglutarate-dependent nucleic acid demethylase. *Science* 2007;**318**:1469–72. https://doi.org/10.1126/science.1151710
17. Li Z, Weng H, Su R *et al.* FTO plays an oncogenic role in acute myeloid leukemia as a N^6-methyladenosine RNA demethylase. *Cancer Cell* 2017;**31**:127–41. https://doi.org/10.1016/j.ccell.2016.11.017
18. Kaklamani V, Yi N, Sadim M *et al.* The role of the fat mass and obesity associated gene (FTO) in breast cancer risk. *BMC Med Genet* 2011;**12**:52. https://doi.org/10.1186/1471-2350-12-52
19. Huff S, Tiwari SK, Gonzalez GM *et al.* m^6A-RNA demethylase FTO inhibitors impair self-renewal in glioblastoma stem cells. *ACS Chem Biol* 2021;**16**:324–33. https://doi.org/10.1021/acschembio.0c00841
20. Zhang S, Zhao BS, Zhou A *et al.* m^6A demethylase ALKBH5 maintains tumorigenicity of glioblastoma stem-like cells by sustaining FOXM1 expression and cell proliferation program. *Cancer Cell* 2017;**31**, 591–606.
21. Guo X, Li K, Jiang W *et al.* RNA demethylase ALKBH5 prevents pancreatic cancer progression by posttranscriptional activation of PER1 in an m^6A-YTHDF2-dependent manner. *Mol Cancer* 2020;**19**:1–19. https://doi.org/10.1186/s12943-020-01158-w
22. Yu H, Yang X, Tang J *et al.* ALKBH5 inhibited cell proliferation and sensitized bladder cancer cells to cisplatin by m^6A-CK2α-mediated glycolysis. *Mol Ther Nucleic Acids* 2021;**23**:27–41. https://doi.org/10.1016/j.omtn.2020.10.031
23. Frayling TM, Timpson NJ, Weedon MN *et al.* A common variant in the FTO gene is associated with body mass index and predisposes to childhood and adult obesity. *Science* 2007;**316**:889–894. https://doi.org/10.1126/science.1141634
24. Dina C, Meyre D, Gallina S *et al.* Variation in FTO contributes to childhood obesity and severe adult obesity. *Nat Genet* 2007;**39**:724–726. https://doi.org/10.1038/ng2048
25. Kivimäki M, Jokela M, Hamer M *et al.* Examining overweight and obesity as risk factors for common mental disorders using fat mass and obesity-associated (FTO) genotype-instrumented analysis: the Whitehall II Study, 1985–2004. *Am J Epidemiol* 2011;**173**:421–429. https://doi.org/10.1093/aje/kwq444
26. Milaneschi Y, Lamers F, Mbarek H *et al.* The effect of FTO rs9939609 on major depression differs across MDD subtypes. *Mol Psychiatry* 2014;**19**:960–2. https://doi.org/10.1038/mp.2014.4
27. Mauer J, Luo X, Blanjoie A *et al.* Reversible methylation of m^6Am in the 5′ cap controls mRNA stability. *Nature* 2017;**541**:371–5. https://doi.org/10.1038/nature21022
28. Mauer J, Sindelar M, Despic V *et al.* FTO controls reversible m^6Am RNA methylation during snRNA biogenesis. *Nat Chem Biol* 2019;**15**:340–7. https://doi.org/10.1038/s41589-019-0231-8
29. Zhang X, Wei L-H, Wang Y *et al.* Structural insights into FTO's catalytic mechanism for the demethylation of multiple RNA substrates. *Proc Natl Acad Sci USA* 2019;**116**:2919–24. https://doi.org/10.1073/pnas.1820574116
30. Wei J, Liu F, Lu Z *et al.* Differential m^6A, m^6Am, and m^1A demethylation mediated by FTO in the cell nucleus and cytoplasm. *Mol Cell* 2018;**71**:973–985. https://doi.org/10.1016/j.molcel.2018.08.011
31. Islam MS, Leissing TM, Chowdhury R *et al.* 2-Oxoglutarate-dependent oxygenases. *Annu Rev Biochem* 2018;**87**:585–620. https://doi.org/10.1146/annurev-biochem-061516-044724
32. Fu Y, Jia G, Pang X *et al.* FTO-mediated formation of N^6-hydroxymethyladenosine and N^6-formyladenosine in

mammalian RNA. *Nat Commun* 2013;**4**:1798. https://doi.org/10.1038/ncomms2822
33. Toh JD, Crossley SW, Bruemmer KJ *et al.* Distinct RNA *N*-demethylation pathways catalyzed by nonheme iron ALKBH5 and FTO enzymes enable regulation of formaldehyde release rates. *Proc Natl Acad Sci USA* 2020;**117**:25284–92. https://doi.org/10.1073/pnas.2007349117
34. Hausinger RP. Fe(II)/α-ketoglutarate-dependent hydroxylases and related enzymes. *Crit Rev Biochem Mol Biol* 2004;**39**:21–68. https://doi.org/10.1080/10409230490440541
35. Loenarz C, Schofield CJ. Physiological and biochemical aspects of hydroxylations and demethylations catalyzed by human 2-oxoglutarate oxygenases. *Trends Biochem Sci.* 2011;**36**:7–18.
36. Rose N, McDonough M, King O *et al.* Inhibition of 2-oxoglutarate dependent oxygenases. *Chem Soc Rev* 2011;**40**:4364–97. https://doi.org/10.1039/c0cs00203h
37. Myllyharju J. In: Schofield C, Hausinger R (eds), *2-Oxoglutarate-Dependent Oxygenases*. Royal Society of Chemistry, 2015, 149–68.
38. Zhang Z, Kochan GT, Ng SS *et al.* Crystal structure of PHYHD1A, a 2OG oxygenase related to phytanoyl-CoA hydroxylase. *Biochem Biophys Res Commun* 2011;**408**:553–8. https://doi.org/10.1016/j.bbrc.2011.04.059
39. Ito S, Shen L, Dai Q *et al.* Tet proteins can convert 5-methylcytosine to 5-formylcytosine and 5-carboxylcytosine. *Science* 2011;**333**:1300–3. https://doi.org/10.1126/science.1210597
40. Falnes PØ, Johansen RF, Seeberg E. AlkB-mediated oxidative demethylation reverses DNA damage in *Escherichia coli*. *Nature* 2002;**419**:178–82. https://doi.org/10.1038/nature01048
41. Kaelin WG, Ratcliffe PJ. Oxygen sensing by metazoans: the central role of the HIF hydroxylase pathway. *Mol Cell* 2008;**30**:393–402. https://doi.org/10.1016/j.molcel.2008.04.009
42. Aas PA, Otterlei M, Falnes PØ *et al.* Human and bacterial oxidative demethylases repair alkylation damage in both RNA and DNA. *Nature* 2003;**421**:859–63. https://doi.org/10.1038/nature01363
43. Chen B, Liu H, Sun X *et al.* Mechanistic insight into the recognition of single-stranded and double-stranded DNA substrates by ABH2 and ABH3. *Mol BioSyst* 2010;**6**:2143–9. https://doi.org/10.1039/c005148a
44. Yang C-G, Yi C, Duguid EM *et al.* Crystal structures of DNA/RNA repair enzymes AlkB and ABH2 bound to dsDNA. *Nature* 2008;**452**:961–5. https://doi.org/10.1038/nature06889
45. Duncan T, Trewick SC, Koivisto P *et al.* Reversal of DNA alkylation damage by two human dioxygenases. *Proc Natl Acad Sci USA* 2002;**99**:16660–5. https://doi.org/10.1073/pnas.262589799
46. Sundheim O, Vågbø CB, Bjørås M *et al.* Human ABH3 structure and key residues for oxidative demethylation to reverse DNA/RNA damage. *EMBO J* 2006;**25**:3389–97. https://doi.org/10.1038/sj.emboj.7601219
47. Yu B, Edstrom WC, Benach J *et al.* Crystal structures of catalytic complexes of the oxidative DNA/RNA repair enzyme AlkB. *Nature* 2006;**439**:879–84. https://doi.org/10.1038/nature04561
48. Kaur S, Tam NY, McDonough MA *et al.* Mechanisms of substrate recognition and N^6-methyladenosine demethylation revealed by crystal structures of ALKBH5–RNA complexes. *Nucleic Acids Res* 2022;**50**:4148–60. https://doi.org/10.1093/nar/gkac195
49. Shishodia S, Zhang D, El-Sagheer A *et al.* NMR analyses on *N*-hydroxymethylated nucleobases—implications for formaldehyde toxicity and nucleic acid demethylases. *Org Biomol Chem* 2018;**16**:4021–32. https://doi.org/10.1039/C8OB00734A
50. Toh JDW, Sun L, Lau LZM *et al.* A strategy based on nucleotide specificity leads to a subfamily-selective and cell-active inhibitor of N^6-methyladenosine demethylase FTO. *Chem Sci* 2015;**6**:112–22. https://doi.org/10.1039/C4SC02554G
51. McGhee JD, Von Hippel PH. Formaldehyde as a probe of DNA structure. II. Reaction with endocyclic imino groups of DNA bases. *Biochemistry* 1975;**14**:1297–303. https://doi.org/10.1021/bi00677a030
52. Zou S, Toh JDW, Wong KHQ *et al.* N^6-Methyladenosine: a conformational marker that regulates the substrate specificity of human demethylases FTO and ALKBH5. *Sci Rep* 2016;**6**:25677. https://doi.org/10.1038/srep25677
53. Zhu Y, Zhou G, Yu X *et al.* LC–MS–MS quantitative analysis reveals the association between FTO and DNA methylation. *PLoS One* 2017;**12**:e0175849. https://doi.org/10.1371/journal.pone.0175849
54. Jia G, Yang C-G, Yang S *et al.* Oxidative demethylation of 3-methylthymine and 3-methyluracil in single-stranded DNA and RNA by mouse and human FTO. *FEBS Lett* 2008;**582**:3313–9. https://doi.org/10.1016/j.febslet.2008.08.019
55. Aik W, Demetriades M, Hamdan MK *et al.* Structural basis for inhibition of the fat mass and obesity associated protein (FTO). *J Med Chem* 2013;**56**:3680–8. https://doi.org/10.1021/jm400193d
56. Aik W, Scotti JS, Choi H *et al.* Structure of human RNA N^6-methyladenine demethylase ALKBH5 provides insights into its mechanisms of nucleic acid recognition and demethylation. *Nucleic Acids Res* 2014;**42**:4741–54. https://doi.org/10.1093/nar/gku085
57. Hopkinson RJ, Tumber A, Yapp C *et al.* 5-Carboxy-8-hydroxyquinoline is a broad spectrum 2-oxoglutarate oxygenase inhibitor which causes iron translocation. *Chem Sci* 2013;**4**:3110–7. https://doi.org/10.1039/c3sc51122g
58. Shishodia S, Schofield CJ. Improved synthesis of phosphoramidite-protected N^6-methyladenosine via BOP-mediated S_NAr reaction. *Molecules* 2020;**26**:147. https://doi.org/10.3390/molecules26010147
59. Shishodia S, Demetriades M, Zhang D *et al.* Structure-based design of selective fat mass and obesity associated protein (FTO) inhibitors. *J Med Chem* 2021;**64**:16609–25. https://doi.org/10.1021/acs.jmedchem.1c01204
60. Han Z, Niu T, Chang J *et al.* Crystal structure of the FTO protein reveals basis for its substrate specificity. *Nature* 2010;**464**:1205–9. https://doi.org/10.1038/nature08921
61. Fiorini G, Marshall SA, Figg WD *et al.* Human prolyl hydroxylase domain 2 reacts with O2 and 2-oxoglutarate to enable formation of inactive Fe(III)·2OG·hypoxia-inducible-factor α complexes. *Sci Rep* 2024;**14**:26162. https://doi.org/10.1038/s41598-024-75761-y
62. Khan A, Schofield CJ, Claridge TDW. Reducing agent-mediated nonenzymatic conversion of 2-oxoglutarate to succinate: implications for oxygenase assays. *ChemBioChem* 2020;**21**:2898–902. https://doi.org/10.1002/cbic.202000185
63. Markolovic S, Leissing TM, Chowdhury R *et al.* Structure–function relationships of human JmjC oxygenases—demethylases versus hydroxylases. *Curr Opin Struct Biol* 2016;**41**:62–72. https://doi.org/10.1016/j.sbi.2016.05.013
64. Ogawa A, Nagiri C, Shihoya W *et al.* N^6-Methyladenosine (m^6A) is an endogenous A3 adenosine receptor ligand. *Mol Cell* 2021;**81**:659–74. https://doi.org/10.1016/j.molcel.2020.12.038
65. Traut TW. Physiological concentrations of purines and pyrimidines. *Mol Cell Biochem* 1994;**140**:1–22. https://doi.org/10.1007/BF00928361
66. Salazar-Cerezo S, Martínez-Montiel N, García-Sánchez J *et al.* Gibberellin biosynthesis and metabolism: a convergent route for plants, fungi and bacteria. *Microbiol Res* 2018;**208**:85–98. https://doi.org/10.1016/j.micres.2018.01.010
67. Baldwin JE, Goh K-C, Schofield CJ. Oxidation of deacetylcephalosporin C by deacetoxycephalosporin C/deacetylcephalosporin C synthase. *J Antibiot* 1992;**45**:1378–81. https://doi.org/10.7164/antibiotics.45.1378
68. Zheng G, He C. In: Schofield C, Hausinger R (eds), *2-Oxoglutarate-Dependent Oxygenases*. The Royal Society of Chemistry, 2015, 263–74. https://doi.org/10.1039/9781782621959

69. Tahiliani M, Koh KP, Shen Y *et al.* Conversion of 5-methylcytosine to 5-hydroxymethylcytosine in mammalian DNA by MLL partner TET1. *Science* 2009;**324**:930–5. https://doi.org/10.1126/science.1170116
70. Fu L, Guerrero CR, Zhong N *et al.* Tet-mediated formation of 5-hydroxymethylcytosine in RNA. *J Am Chem Soc* 2014;**136**:11582–5. https://doi.org/10.1021/ja505305z
71. Li Y, Wu K, Quan W *et al.* The dynamics of FTO binding and demethylation from the m^{6}A motifs. *RNA Biol* 2019;**16**:1179–89. https://doi.org/10.1080/15476286.2019.1621120
72. Yu J, Chen M, Huang H *et al.* Dynamic m^{6}A modification regulates local translation of mRNA in axons. *Nucleic Acids Res* 2018;**46**:1412–23. https://doi.org/10.1093/nar/gkx1182
73. Tang C, Klukovich R, Peng H *et al.* ALKBH5-dependent m^{6}A demethylation controls splicing and stability of long 3′-UTR mRNAs in male germ cells. *Proc Natl Acad Sci USA* 2018;**115**:E325–33. https://doi.org/10.1073/pnas.1717794115
74. Jiang X, Liu B, Nie Z *et al.* The role of m^{6}A modification in the biological functions and diseases. *Signal Transduct Target Ther* 2021;**6**:74. https://doi.org/10.1038/s41392-020-00450-x
75. Chen X, Chothia SY, Basran J *et al.* Formaldehyde regulates tetrahydrofolate stability and thymidylate synthase catalysis. *Chem Commun* 2021;**57**:5778–81. https://doi.org/10.1039/D1CC01425K
76. John T, Saffoon N, Walsby-Tickle J *et al.* Aldehyde-mediated inhibition of asparagine biosynthesis has implications for diabetes and alcoholism. *Chem Sci* 2024;**15**:2509–17. https://doi.org/10.1039/D3SC06551K
77. Schofield C, Hausinger R (eds), *2-Oxoglutarate-Dependent Oxygenases*. The Royal Society of Chemistry, 2015. https://doi.org/10.1039/9781782621959
78. Thalhammer A, Bencokova Z, Poole R *et al.* Human AlkB homologue 5 is a nuclear 2-oxoglutarate dependent oxygenase and a direct target of hypoxia-inducible factor 1α (HIF-1α). *PLoS One* 2011;**6**:e16210. https://doi.org/10.1371/journal.pone.0016210
79. Wang X, Sun H, Cui L *et al.* Acute high-altitude hypoxia exposure causes neurological deficits via formaldehyde accumulation. *CNS Neurosci Ther* 2022;**28**:1183–94. https://doi.org/10.1111/cns.13849
80. Dong F, Qin X, Wang B *et al.* ALKBH5 facilitates hypoxia-induced paraspeckle assembly and IL8 secretion to generate an immunosuppressive tumor microenvironment. *Cancer Res* 2021;**81**:5876–88. https://doi.org/10.1158/0008-5472.CAN-21-1456
81. Benak D, Sevcikova A, Holzerova K *et al.* FTO in health and disease. *Front Cell Dev Biol* 2024;**12**:1500394. https://doi.org/10.3389/fcell.2024.1500394
82. Hubacek JA, Pikhart H, Peasey A *et al.* The association between the FTO gene variant and alcohol consumption and binge and problem drinking in different gene–environment background: the HAPIEE study. *Gene* 2019;**707**:30–5. https://doi.org/10.1016/j.gene.2019.05.002

Received: March 17, 2025. **Revised:** June 12, 2025. **Editorial Decision:** July 13, 2025. **Accepted:** August 7, 2025